Interfacial Strength Evaluation between Sulfur-segregated Al_2O_3 and Ni-Al Single Crystal Alloy Using Nanoindentation

Chihiro Tabata[1,2,*], Toshio Osada[1], Takahito Ohmura[1], Tadaharu Yokokawa[1], Kyoko Kawagishi[1,2], and Shinsuke Suzuki[2,3,4]

1. National Institute for Materials Science (NIMS), 1-2-1 Sengen, Tsukuba, Ibaraki 305-0047, Japan
2. Department of Materials Science, Waseda University,3-4-1 Okubo, Shinjuku-ku, Tokyo 169-8555, Japan
3. Department of Applied Mechanics and Aerospace Engineering, Waseda University, 3-4-1 Okubo, Shinjuku-ku, Tokyo 169-8555, Japan
4. Kagami Memorial Institute for Materials Science and Technology, Waseda University, 2-8-26 Nishiwaseda, Shinjuku-ku, Tokyo 169-0051, Japan

*Corresponding author: chihiro448@akane.waseda.jp (C. Tabata)

Keywords: Nanoindentation, Oxidation, Sulfur segregation, Interfacial strength, Ni-base single crystal alloy

Abstract

Ni-base superalloys have excellent oxidation resistance, but impurity S drastically decreases their properties. This is due to the segregation of S to the oxide/substrate interface, but direct and quantitative measurements of the interfacial strength in relation to the S segregation level have not been widely conducted. The objective of this research is to quantitatively analyze the interfacial strength between the Al_2O_3 layer and Ni-base substrate interfacial strength, depending on the S segregation level, using nanoindentation. Ni-9.8 wt.% Al alloys were prepared by melting the material using either an Al_2O_3 crucible (high $S_{interface}$ alloy) or a CaO crucible (low $S_{interface}$ alloy). Nanoindentation tests using a 60 degree pyramidal diamond indenter were conducted, and the cross-sections of both specimens exposed the (100) plane. Indentation near the interface formed cracks at the boundary between the two layers, which can be observed as pop-ins in the load-depth curves. The amount of load at the initial pop-in most likely represents the interfacial strength between the Al_2O_3 layer and Ni-base substrate. A Weibull analysis of results showed that suppression of the S segregation level increased the critical β scale parameter for crack formation by 650 μN. This suggests that we were able to successfully compare the effect of S segregation on the interfacial strength between the Al_2O_3 layer and the Ni-base substrate quantitatively.

Introduction

Ni-base single-crystal superalloys are designed to have excellent oxidation resistance and mechanical properties at high temperatures of about 1000 °C. To improve the thermal efficiency of jet engines and gas turbines, single-crystal superalloys such as TMS-238, which has temperature capabilities higher than 1100 °C, has been created [1]. For these superalloys, cyclic oxidation resistance plays an important role. However, impurities such as S, which enter the alloys from the fuel and the environment used, are known to be detrimental to the high temperature oxidation, even at a ppm level [2-8]. This is most likely caused by decrease in the adhesion of the interface between the Al_2O_3 oxide layer and the Ni-base substrate, due to the S segregation at this interface. To avoid any S segregation, according to Smialek, the ideal S concentration without the addition of reactive elements would be around 0.1 ppm; for wall thickness relevant to turbine components, it needs to be <1 ppm to observe oxidation benefit [6].

Additionally, with the rise in the cost of rare metals, methods to reuse materials will be required, and techniques to remove impurity S will be crucial. Utada *et al.* developed the direct recycling method which uses CaO crucibles rather than the conventional Al_2O_3 crucibles to remelt the used turbine blades, made of Ni-base superalloys [9]. This not only removes the S from the alloy, but also limits the S segregation level at the Al_2O_3/alloy interface by trapping S within the substrate by the formation of CaS, thus improving its oxidation resistance [7,8]. Using this method, we were able to see improvement in oxidation resistance even for alloys with S content higher than 1 ppm, due to the decrease in the S segregation level at the interface observed using scanning transmission electron microscopy with energy-dispersive X-ray spectroscopy (STEM-EDS) and 3D atom probe (3DAP) [7,8]. These results suggest that the critical factor is the S segregation level at the interface, rather than the S concentration of the alloy.

Therefore, to determine the S segregation level acceptable for creating oxidation resistant alloys from both ingots and reused materials, it is important to analyze the oxide/substrate interfacial strength quantitatively. Several authors reported that calculations and simulations had made it possible to predict the differences in interfacial strength caused by S segregation. For example, density functional theories have been used by several researchers to determine the changes in adhesion of Al_2O_3 layer and Ni-base substrate by the existence of S [10-12]. Other methods such as macroscopic atom models have also been used by Bennett *et al.* to determine the adhesion of oxides and metals [13]. However, this has been difficult to quantify the segregation level and the changes in interfacial strength, as well as proving these results experimentally. Scratch or pull-off tests have been used previously to assess the adhesion of oxide layers [6,14-15]. Hou *et al.* determined the S segregation level using Auger electron spectroscopy and compared the interfacial strength using Vickers micro-indenters and tensile testers [4,16]. They have shown that the oxide/substrate interface had weakened due to the existence of S. But these methods are difficult to use when trying to compare the differences directly and quantitatively for the interfacial strengths caused by the S, specifically at the Al_2O_3/alloy, due to the sizing and adherence of the interface and the formation of various layers of oxides.

Therefore, the objective of this research is to incorporate nanoindentation to quantitatively clarify the interfacial strength between the Al_2O_3 layer and the Ni-base substrate, depending on the S segregation level. Several factors such as the placement of the indenters within the specimens as well as the reliability of the tests were considered, and what had occurred during the nanoindentation tests was analyzed as well.

Experimental Methods

Ni-9.8 wt.% Al single crystal (SC) alloys, used in a previous study [8], were also used for this research to simplify the interfacial structure by constraining the oxide species formed, while retaining similar γ/γ' structures as the Ni-base superalloys. Alloys with different levels of S segregation at the interface were created by melting the materials using an Al_2O_3 crucible (alloy (high $S_{interface}$)), and a CaO crucible (alloy (low $S_{interface}$)). The alloys contained 2 ppm of S and <1 ppm of Ca for alloy (high $S_{interface}$), and 3 ppm of S and 6.2 ppm of Ca for alloy (low $S_{interface}$), both of which were mirror polished and chemically analyzed using glow discharge mass spectrometry [8]. Although the S contents were about the same, S segregation level at the interface between Al_2O_3 and Ni-Al alloy was significantly higher for alloy (high $S_{interface}$) compared to alloy (low $S_{interface}$) [8]. In the previous research the samples were oxidized at 1100°C for 1 h and cooled in air, and the S segregation levels were measured using STEM-EDS, during which, the alloy (high $S_{interface}$) had around 2.0 at.% S segregation at the interface, while the alloy (low $S_{interface}$) showed less than 0.5 at.% S segregation. Note that how much S segregation is present at the scale-metal interface depends on the S reservoir, which is proportional to metal thickness, and the time and temperature exposed, all of which were consistent between the two types of samples. Separate samples created from the same ingot were prepared for nanoindentation measurements. To match the conditions to the previous research and to grow the Al_2O_3 scale and limit the oxide spallation as much as possible, the specimens were oxidized at 1100 °C for 1 h in air and cooled off within the furnace at 10 °C/min. Each specimen was cut into a cuboid with 5 mm in height and placed on an Al-based platform so that the Al_2O_3/alloy interface faced upwards. The crystal orientations of the specimens were measured using the Laue X-ray backscattering method (RIGAKU SA-HF3S) and adjusted so that all specimens faced the (100) plane during testing. The cross-sections of each specimen were both mirror and vibration polished (Saphir Vibro, ATM).

Nanoindentation (HYSITRON, TI950 TriboIndenter) tests were conducted to measure the differences in the interfacial strength of the alloys, using a diamond, 3-sided pyramid tip with an angle of 60 degrees. Figure 1 shows the schematic diagram of the nanoindentation tests conducted for both alloy (high $S_{interface}$) and alloy (low $S_{interface}$) in this research. The initial indent position was in the Al_2O_3 oxide layer, 0.5 μm away from the interface of the protective oxide layer and Ni-base alloy for testing at the interface (Fig. 1(b)). This is far enough from the interface so that the cracks forms between the two layers during testing, but not too far so that the indenter does not fall within the Al_2O_3 layer. Only for the Al_2O_3 layer, initial indent positions were set at around 1.0 nm away from the interface (Fig. 1(a)). Tests were also conducted within the substrate as well (Fig. 2(c)). The distance was determined by the observation of the

oxide/substrate interface using atomic force microscopy, where the microscope was incorporated within the TI950 TriboIndenter. The tests conducted near the interface were executed 17 times for each specimen, where each test was conducted at 600 μN/s loading and unloading rate and 10 s holding time in between (only for test conducted directly at the interface in the discussion section, it was conducted at 750 μN/s loading and unloading rate and 10 s holding time in between). Scanning Electron Microscope (SEM) images of each indentation marks were taken afterwards using field emission scanning electron microscope (FE-SEM, ZEISS GeminiSEM300). Electron backscatter diffraction (EBSD, ZEISS GeminiSEM300) maps were taken at the interface of both specimens as well.

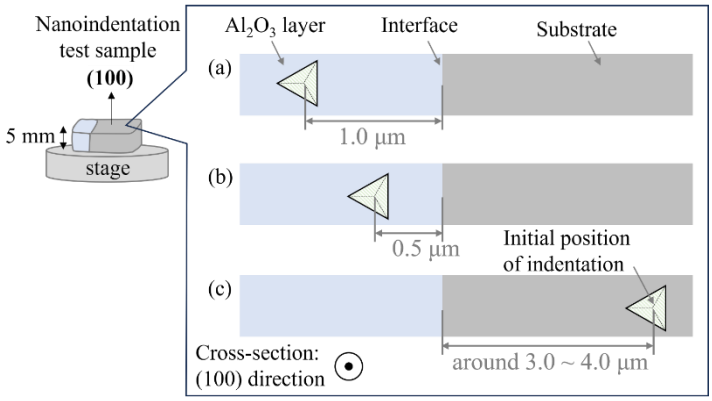

Figure 1 – Schematic diagram of the nanoindentation test sample and the position of indentation for testing at (a) Al_2O_3 layer, (b) interface, and (c) substrate.

Results

Figure 2 (a) shows an example of load (P)-penetration depth (h) curves of alloy (low $S_{interface}$), tested within the Al_2O_3 layer, near the Al_2O_3/alloy interface, and on the Ni-Al alloy. The white plots within the SEM images are the locations of where the indenters were placed initially. For indentation near the interface, deformation by the nanoindentor started off within the Al_2O_3 layer, resulting in the same slope as the curves for the Al_2O_3 oxide layer. The large strain burst event, called a 'pop-in', is triggered by crack formation on the interface as shown in the SEM image. This load is surmised to correspond to interfacial cracking of the alloy, since there appears a significantly higher pop-in load for the indents within the Al_2O_3 layer. In this study, the initial pop-in load (P_c) was determined to be an indicator of interfacial strength. Further, after the large initial pop-in on interface, the indent tip moved from initial position to the alloy. Due to the tip movement, the slope of P-h curve near the interface significantly decreased compared to before the pop-in and exhibited a shallower slope than that on the alloy. Furthermore, the P-h curve included several small pop-in events. Thus, the decreased slope includes both alloy deformation and crack propagations.

Figure 2 (b) shows the results for the same tests conducted on alloy (high $S_{interface}$). The P_c taken from the tests conducted within the Al_2O_3 was 5503 μN for alloy (high $S_{interface}$) and 5671 μN for alloy (low $S_{interface}$),

and the curves are similar in shape. The same shift in the *P-h* curve could be observed in both Figs. 2 (a) and (b), showing that this test could be conducted for both alloys. The occurrence of pop-in was judged by a rapid increase of penetration depth under nearly constant load. The rapid increase was judged by the criterion that the increase of the penetration depth Δh from the previous plot was larger than 1.0 nm (3.0 nm only for Al_2O_3 layer). This was done to eliminate the effect of small crack formations at the beginning of the test, most likely effects from the porous Ni-Al-O layer formed nearby.

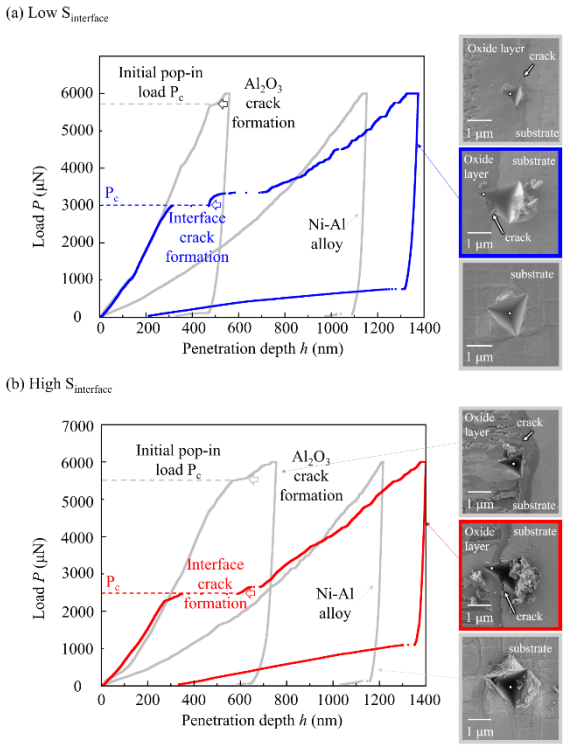

Figure 2 – *P-h* curves of (a) Al_2O_3 layer (gray line on left), interface (blue), and alloy (gray line on the right) for Ni-Al melted using a CaO crucible (low $S_{interface}$). (b) Al_2O_3 layer (gray line on left), interface (red), and alloy (gray line on right) for Ni-Al melted using an Al_2O_3 crucible (high $S_{interface}$).

Figure 3 shows five *P-h* curves near the interface for (a) alloy (high $S_{interface}$) and (b) alloy (low $S_{interface}$), and one of the SEIs after the indentation tests. The crack lengths associated with the indents were slightly larger for alloy (high $S_{interface}$) compared to alloy (low $S_{interface}$), and all test results showed crack formation at the Al_2O_3/alloy interface. This suggests that the method is reproducible for detecting interfacial cracking events. Further, P_c for alloy (high $S_{interface}$) is lower than that for alloy (low $S_{interface}$). However, P_c for both alloy (high $S_{interface}$) and (low $S_{interface}$) show large scatters because of the brittle fracture on the interface. These results suggest that the Al_2O_3/alloy interfacial strength was lower for alloy (high $S_{interface}$) than alloy (low $S_{interface}$).

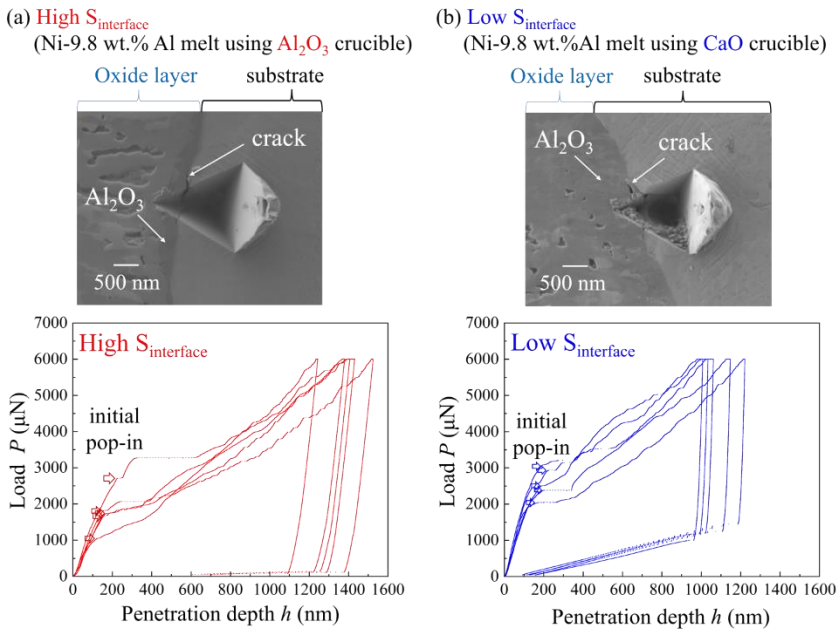

Figure 3– SEIs of the indentation marks and load-depth curves for (a) Ni-Al melted using an Al_2O_3 crucible (alloy (high $S_{interface}$)) and (b) Ni-Al melted using CaO crucible (alloy (low $S_{interface}$)). Arrows show where the initial pop-in had occurred.

Discussion

To statistically evaluate the differences in P_c for brittle interfacial cracking of the two alloys, P_c values were evaluated based on two-parameter Weibull distributions as shown in Figure 4. Here, the median ranking method; $F(P_c) = i - 0.3/N + 0.4$, where i is the P_c order, and N is the number of tests, was used. The Weibull equation is as follows:

$$\ln\ln\frac{1}{1-F(P_c)} = m(\ln P_c - \ln\beta) \quad (1)$$

where m is the Weibull parameter, and β is the scale parameter. The slope and intercept of approximated linear lines shown for each alloy in Fig. 4 are used to determine m- and β-values. The red triangles represent the results for alloy (high $S_{interface}$), and the blue squares represent the results for alloy (low $S_{interface}$). For alloy (high $S_{interface}$), $m = 3.48$, and $\beta = 2248$ μN, while for alloy (low $S_{interface}$), $m = 6.39$, and $\beta = 2898$ μN. The values of the coefficient of determination were 0.958 and 0.989, respectively, indicating that both linear lines are well-fitted. This implies that alloy (high $S_{interface}$), which has higher S segregation at the interface between Al_2O_3 layer and Ni-base substrate, shows significantly lower strength and larger scatter than low S interface. Therefore, it can be said that alloy (low $S_{interface}$) had 650 μN higher P_c compared to alloy (high $S_{interface}$), which also directly relates to the interfacial strength between the Al_2O_3 layer and Ni-base substrate, due to the suppression of S segregation. The m- and β-values consider the effect of not only the interfacial strength but also the shape of the interface and the location of initial indent position as well.

However, the shape of interface and the locations of initial indent position were selected to be about the same for each test. Therefore, the effects are most likely small and significant differences were observed in the pop-in load (P_c), making this test method effective for differentiating interfacial strength, most likely for superalloys as well.

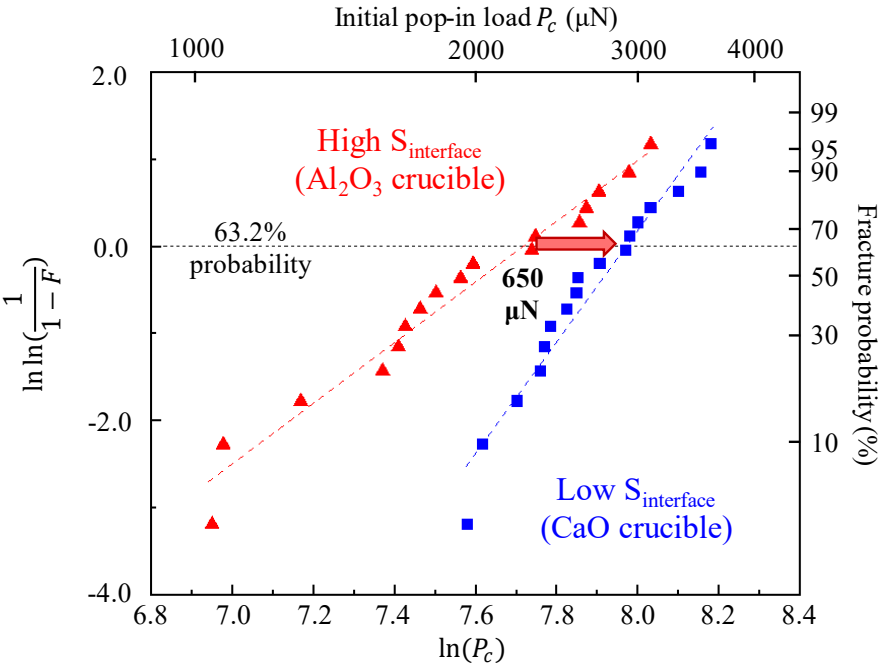

Figure 4 – Weibull plots of the initial pop-in with Δh larger than 1.0 nm for Ni-Al alloys with different interfacial S segregation level. The red triangles indicate the results for Ni-Al melted using an Al_2O_3 crucible (alloy (high $S_{interface}$)), and the blue squares represents the results for Ni-Al melted using a CaO crucible (alloy (low $S_{interface}$)).

Next, the most likely process during this test was evaluated. When the indentation is conducted directly at the interface, it proved difficult to form cracks between the two layers. Figure 5 shows the (a) SEM image and (b) the *P-h* curve of when nanoindentation was conducted directly at the interface of the Al_2O_3 layer and Ni-base substrate for the alloy (low $S_{interface}$). Here, large crack formation can be seen within the Al_2O_3 layer; however, pop-in events cannot be observed in the *P-h* curve. It is evident that the indenter has slid towards the substrate before creating a clear indent at the interface. This is most likely due to the difference in the relative hardness of the two layers which were 13.7 GPa for Al_2O_3 and 3.64 GPa for the substrate, respectively. The *P-h* curve is similar to that taken at the substrate in Figs. 2 (a) and (b), suggesting that the test took place mostly in the substrate. From this result we can assume that the indenter has the tendency to deviate towards the substrate.

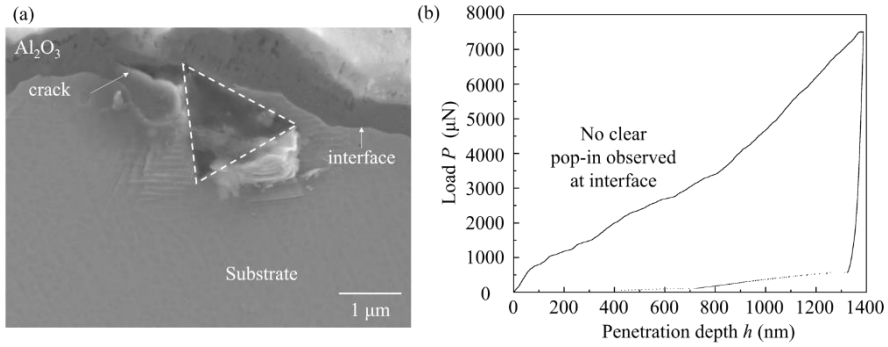

Figure 5 – Results of nanoindentation test conducted directly at the interface. (a) SEI of indentation mark conducted directly at the interface for alloy (low $S_{interface}$) with the white dotted lines representing the indent perimeter and (b) the load-depth curve of this result.

Several factors may affect these nanoindentation test results. For example, the crystal orientations and grain sizes of the Al_2O_3, as well as the thickness of these layers may alter the P_c values. To evaluate such points, EBSD analyses were conducted at the interface of both alloy (high $S_{interface}$) and alloy (low $S_{interface}$). Figure 6 shows the crystal orientations of the Al_2O_3 grains and the substrate of both alloy (high $S_{interface}$) and alloy (low $S_{interface}$). The substrate, which is the bottom half of the figures, faces the (100) direction for both alloys and are shown in red. The small grains shown in the top half of the images most likely represents the Ni-Al-O layers. The Al_2O_3 grains, shown right on top of the substrate, are around 1 μm in width and between 0.4 and 0.7 μm height for both alloys, showing that the size of these grains is similar for both alloys. The crystal orientations for these grains, however, varies greatly. But for this research, the same indentation tests were conducted several times at different locations. By comparing the results using Weibull distribution, the differences caused by the crystal orientations of Al_2O_3 are incorporated into the results. We also assume that there may be a range of values with the increase in monolayers of S at the interface. However, factors such as these Al_2O_3 crystal orientations will also affect the results, and currently it is difficult to distinguish which factors affect the values of the interfacial strength the most. Therefore, this is also something to consider for future works.

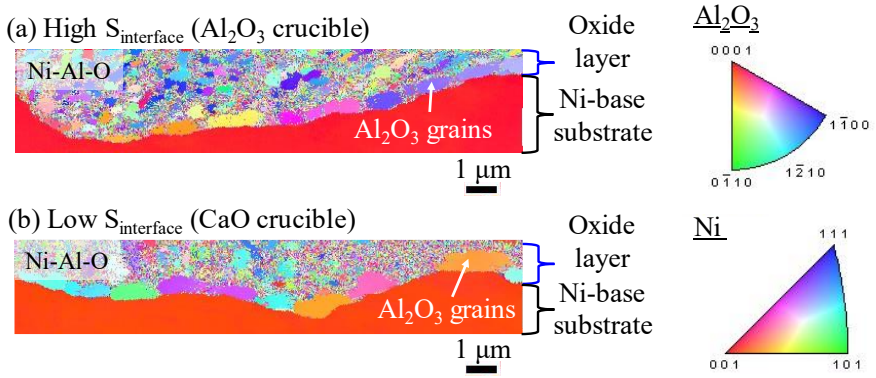

Figure 6 – EBSD crystal orientation maps of Al_2O_3 and Ni-base substrate taken at the interface of (a) alloy (high $S_{interface}$) and (b) alloy (low $S_{interface}$).

Figure 7 shows the schematic diagram depicting what is most likely occurring during these nanoindentation tests; (a) the schematic *P-h* curve, (b) the top view, and (c) the side view of the tests conducted. (i) At the beginning of the test, indenter is placed on the oxide layer, 0.5 μm away from the interface. (ii) The indenter penetrates within the oxide, creating stress regions shown in yellow. (iii) The stress gradually increases as the indenter penetrates deeper within the sample. Before the indenter itself reaches the interface, stress will be applied to the interface indirectly. This will most likely lead to crack formations at the interface. (iv) Because the substrate is mostly γ phase due to the Al depletion by oxidation, it easily deforms compared to the Al_2O_3 oxide layer, which is ceramic, and the indenter gradually slides toward the interface. The indenter is pushed onto the interface, leading to the growth of the crack at the interface. When the indent size increased enough in *h* and the indenter edge with high stress concentration approached the interface, pop-in event is observed in the *P-h* curves. Afterwards, the indenter will continue moving towards the substrate, leading to the large pile-up at the end.

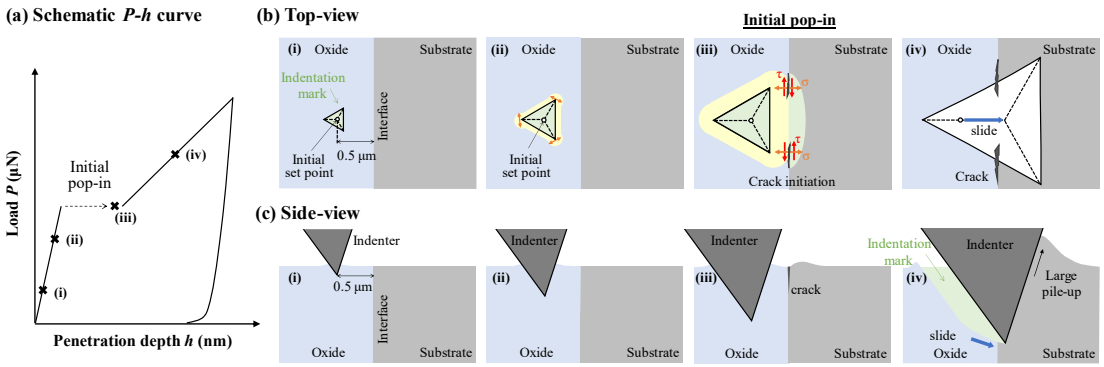

Figure 7 – Schematic diagram of (a) load-depth curve, (b) top-view and (c) side-view of the nanoindentation test conducted near the interface.

Conclusions

To conclude, the following have been clarified regarding the measurement of the interfacial strength between the Al_2O_3 layer and Ni-base substrate of the two types of Ni-9.8 wt.% Al alloys; an alloy melted using an Al_2O_3 crucible (high $S_{interface}$) and an alloy melted using a CaO crucible (low $S_{interface}$):

1. Nanoindentation tests were conducted so that the side of the triangular indenter was parallel to the interface of the Al_2O_3 layer and Ni-base substrate. The indenter was placed on the Al_2O_3 layer, 0.5 μm away from the interface, since placing it directly at the interface causes the indenter to slide towards the substrate before crack formation. The large difference in the hardness most likely leads to this phenomenon.
2. Clear differences in the interfacial strength between alloys were observed using nanoindentation. According to the *P-h* curves, alloy (high $S_{interface}$), which has higher S segregation level at the interface of the Al_2O_3 layer and Ni-base substrate, showed that the initial pop-in load, P_c, was lower compared to alloy (low $S_{interface}$). The tests conducted near the interface, within Al_2O_3, and on the substrate showed that the pop-in seen in the *P-h* curves most likely represents the crack initiation at the interface.
3. The Weibull distributions showed that alloy (low $S_{interface}$) had 650 μN higher median pop-in load than alloy (high $S_{interface}$), due to the suppression of the S segregation level. The fitted linear lines showed high coefficient of determination values, indicating that the values are reliable. This method can directly compare the interfacial strength quantitatively and is most likely suitable for the measurement of complex superalloys as well.

We also plan on testing using TMS-238, a sixth generation Ni-base single crystal superalloy, since the S segregation level has been measured using 3DAP and STEM-EDS in previous research [7]. Ideally, the nanoindentation tests should also be conducted at elevated temperatures, to recreate the high temperature conditions and the effects of cyclic oxidation. However, that will be for future work.

Acknowledgements

This research was financially supported by Grant-in-Aid for JSPS Fellows Grant Number 23KJ2024. This paper is also based on results obtained from a project, JPNP21007, commissioned by the New Energy and Industrial Technology Development Organization (NEDO). The authors would like to express our gratitude to Dr. Makoto Osawa for the helpful discussions. We also would like to thank Mr. Yuji Takata for the preparation of the single crystal alloys, Mr. Takuma Kohata for the SEM observations, and Ms. Eri Nakagawa for assisting the nanoindentation tests.

References

[1] Kawagishi K, Yeh AC, Yokokawa T, Kobayashi T, Koizumi Y, Harada H (2012) Development of an oxidation-resistant high-strength sixth-generation single-crystal superalloy TMS-238, Superalloys 2012. 189-195. doi: 10.1002/9781118516430

[2] Smith MA, Frazier WE, Pregger BA (1995) Effect of sulfur on the cyclic oxidation behavior of a single crystalline, nickel-base superalloy. Mater. Sci. Eng. A. 203:388-398. doi:10.1016/0921-5093(95)09819-4

[3] Molins R, Rouzou I, Hou P (2007) A TEM study of sulfur distribution in oxidized Ni40Al and its effect on oxide growth and adherence. Mater. Sci. Eng. A. 454-455:80-88. doi:10.1016/j.msea.2006.11.015

[4] Hou PY, Izumi T, Gleeson B (2009) Sulfur Segregation at Al2O3/γ-Ni + γ′-Ni3Al Interfaces: Effects of Pt, Cr and Hf Additions. Oxid. Met. 72:109-124. doi: 10.1007/s11085-009-9149-y

[5] Fedorova E, Monceau D, Oquab D (2010) Quantification of growth kinetics and adherence of oxide scales formed on Ni-based superalloys at high temperature. Corros. Sci. 52:3932-3942. doi:10.1016/j.corsci.2010.08.013

[6] Smialek JL (2022) Invited Review Paper in Commemoration of Over 50 Years of Oxidation of Metals: Alumina Scale Adhesion Mechanisms: A Retrospective Assessment. Oxid. Met. 97:1-50. doi: 10.1007/s11085-021-10091-2

[7] Tabata C, Kawagishi K, Uzuhashi J, Ohkubo T, Hono K, Yokokawa T, Harada H, Suzuki S (2021) Quantitative analysis of sulfur segregation at the oxide/substrate interface in Ni-base single crystal superalloy. Scr. Mater. 194:113616. doi:10.1016/j.scriptamat.2020.11.003

[8] Tabata C, Kawagishi K, Uzuhashi J, Ohkubo T, Yokokawa T, Harada H, Suzuki S (2022) Unveiling the Mechanism of Improved Oxidation Resistance for CaO Crucible Melting Using Ni-Al Alloy. Metall. Mater. Trans. A. 53A:2452-2458. doi: 10.1007/s11661-022-06678-2

[9] Utada S, Joh Y, Osawa M, Yokokawa T, Sugiyama T, Kobayashi T, Kawagishi K, Suzuki S, Harada H (2018) Creep Property and Phase Stability of Sulfur-Doped Ni-Base Single-Crystal Superalloys and Effectiveness of CaO Desulfurization. Metall. Mater. Trans. A. 49A:4029-4041. doi: 10.1007/s11661-018-4710-4

[10] Jarvis EA, Carter EA (2002) The role of reactive elements in thermal barrier coatings. Comp. Sci. Eng. 4(2):33-41. doi: 10.1109/5992.988645

[11] Carling KM, Carter EA (2007) Effects of segregating elements on the adhesive strength and structure of the α-Al2O3/β-NiAl interface. Acta Mater. 55(8):2791-2803. doi: 10.1016/j.actamat.2006.12.020

[12] Zhang Z, Zhang RF, Legut D, Li DQ, Zhang SH, Fu ZH, Guo HB (2016) Pinning effect of reactive elements on adhesion energy and adhesive strength of incoherent Al2O3/NiAl interface. Phys. Chem. Chem. Phys. 18:22864. doi:10.1039/c6cp03609k

[13] Bennett IJ, Kranenburg JM, Sloof WG (2005) Modeling the Influence of Reactive Elements on the Work of Adhesion between Oxides and Metal Alloys. J. Am. Ceram. Soc. 88(8):2209-2216. doi:10.1111/j.1551-2916.2005.00408.x

[14] Hou PY, Stringer J (1992) Oxide scale adhesion and impurity segregation at the scale/metal interface. Oxid. Met. 38:323-345. doi: 10.1007/BF00665658

[15] Hou PY, Tolpygo VK (2007) Examination of the platinum effect on the oxidation behavior of nickel-aluminide coatings. Surf. Coat. Tech. 202(4-7):623-627. doi:10.1016/j.surfcoat.2007.06.013

[16] Hou PY, Priimak K (2005) Interfacial Segregation, Pore Formation, and Scale Adhesion on NiAl Alloys. Oxid. Met. 63:113-130. doi: doi.org/10.1007/s11085-005-1954-3